LANDTECHNIK 76(4), 2021, 142–154

DOI:10.15150/lt.2021.3271

LANDTECHNIK
AGRICULTURAL ENGINEERING

A practice-optimized method for measuring the rolling resistance of tractor tires

Julian Schwehn, Valentin Ernst, Stefan Böttinger

Looking at the increased requirements for efficient energy use in agricultural machinery, the optimization of the tire-ground interaction of tractors represents an opportunity to increase the efficiency. Measurements of the rolling resistance on tractor tires are predominantly carried out on single wheels with corresponding test rigs (single wheel tester, flat belt test bench, roller test bench). Currently, only a few characteristic values are available for modern tractor tires. The subject of this research is the determination of the rolling resistance on the overall vehicle. Therefore, the measurement methodology of coast-down tests coming from car sector is applied on a tractor. In addition to the theoretical derivation, the test setup, its implementation and the results are discussed in the context of previous research activities. The results show that the coast-down test is a suitable method for determining the rolling resistance of modern tractor tires in a time-efficient yet precise manner.

Keywords:
Efficiency, tires, rolling resistance, tractor, transport, coast-down tests

In addition to reducing greenhouse gas emissions by at least 40% compared to the reference year 1990, the framework of the European energy and climate policy requests for an increase in energy efficiency of at least 32.5% by 2030 (Europäische Kommission 2018). In its energy and climate targets, the German government also defines a 55% reduction in overall emissions by 2030 compared to 1990. In the agricultural sector, emissions are to be reduced by 34% by 2030 compared to the reference year (Bundesministerium für Umwelt, Naturschutz und nukleare Sicherheit 2019). In the past, the reduction of climate-relevant gases in agricultural machinery was enforced analogously to the automotive sector, primarily through the successive tightening of emissions legislation for mobile machinery (VDMA e.V. 2017). Further major progress is not expected in this area, as corresponding potential is already being exploited. As an alternative to legislative requirements, optimization options within agricultural processes are therefore coming into focus. To this end, options for reduction along the entire process chain were simulated in the joint project EKoTech (Efficient fuel use in agricultural technology) by means of a process and machine model and analysed with regard to fuel consumption (Decker und Frerichs 2016). One sub-sector in this context is agricultural transport, the share of which has increased continuously in recent years. This has resulted in new focus points in the development of tractor tires in regard to the interaction between tires and the ground (Reckleben et al.) with competing demands on the tire tread in the field and on the road. During fieldwork, large tractive forces are to be transmitted with maximum efficiency while protecting the ground. Low tire pressures used for this purpose lead to an increase in the contact area between the tire and the ground. On the road, the focus is on reducing the rolling resistance by increasing the tire pressure. This affects the dynamic properties of the tire, which are important for optimizing driving dynamics

received 8 July 2020 | accepted 20 April 2021| published 3 December 2021

and ride comfort. Therefore, adjusting the tire pressure is the preferred possibility for optimization. Low tire pressures lead to greater deformation of the tire shoulder and the tire sidewall. The increase in flexing losses results in higher rolling resistance, which has to be compensated with additional fuel consumption. The tests described below demonstrate the general transferability of the methodology from the car sector to agricultural machinery. Both, single vehicles and vehicle combinations can be tested. The method allows a very fast relative comparison between different agricultural tires used in practice. In addition, the high time efficiency of the method allows a wide range of configurations to be carried out, such as variations in tire pressure or ballasting. In this way, detailed knowledge of the influences on rolling resistance can be obtained. This also supports the creation of a broad database for modern agricultural tires that can be used in science or research and development.

The rolling resistance is fundamentally dependent on tire design, tire dimensions, wheel load, tire pressure, driving speed and temperature. In the past, the influence of the driving speed on the rolling resistance has repeatedly led to controversial statements in measurements on individual wheels. In his dissertation, Barrelmeyer (1996) conducted tests on asphalt with the Hohenheim single wheel tester (tire dimension 520/70 R 34) and found an influence of wheel load on rolling resistance, but no influence of driving speed. Only with very high wheel loads and on yielding ground, rolling resistance rises with increasing driving speed (Barrelmeyer 1994). In his dissertation, Schulze Zumkley (2017) draws on the findings of Barrelmeyer (1996) and Mitschke and Wallentowitz (2014) and assumes that the speed has no influence on the rolling resistance. Plesser (1997), on the other hand, concludes in his dissertation after tests on a 480/70 R 34 tire using the Hohenheim flat belt test bench that rolling resistance increases with driving speed. He explains it with the increased deformation speed of the viscoelastic tire material. The repetition with a second tire of the dimension 16.9 R 34 shows the same tendency. Current measurements with a tire of the dimension 600/65 R 28 using the Hohenheim single wheel tester show a clear correlation between increasing driving speed and increasing rolling resistance only at high wheel loads above 25 kN. Measurements at low wheel loads up to 20 kN are characterized by a strong scattering of the individual measurements (Fery 2019). Rolling resistance measurements on the overall vehicle are only known from the passenger car and commercial vehicle sectors, although Bode and Bode (2013) also points to contrary trends in the commercial vehicle sector. In the agricultural technology sector, measurements on the complete vehicle have not been published yet.

Test method

The theoretical basis for the coast-down test is provided by a balance of forces for a vehicle during transient driving ($v \neq$ konst.) using driving resistance forces. The total resistance force F_{FW} of the vehicle results from the air resistance F_L, the rolling resistance of the wheels F_R, the gradient resistance F_{St} of the road, the acceleration resistance due to the mass inertia of the vehicle F_B and the drag resistance force of the drive train F_A (equation 1):

$$F_{FW} = F_L + F_R + F_{St} + F_B + F_A \qquad \text{Eq. (1)}$$

The air resistance of the tractor is represented by equation 2. In addition to the quadratic dependence on the incoming flow velocity, the air resistance is influenced by values that can be assumed constant during the measurements. These include the flow resistance coefficient c_W, the projected frontal area A and the density of air ρ_L. In general, no wind is assumed, so that the incoming flow velocity corresponds to the vehicle speed v.

$$F_L = c_W \cdot A \cdot \frac{\rho_L}{2} \cdot v^2 \qquad \text{Eq. (2)}$$

The rolling resistance F_R on the overall vehicle consists of an inner and an outer component. The external rolling resistance results from the deformation of the road surface (tracking, etc.) and is neglected for solid roads. The inner rolling resistance results mainly from the flexing losses due to the viscoelastic properties of the tire material. The share of flexing losses in the internal rolling resistance is between 80 and 95% (Heissing et al. 2013). The remaining proportion is accounted for friction and sliding processes between the tire slack and the surface of the road. The rolling resistance force is calculated from equation 3, which relates the rolling resistance coefficient f_R and the normal force. The normal force is calculated from the mass of the vehicle m, the gravitational constant g and the gradient angle α. This results from the slope of the roadway and is calculated in the test from the change in height of the vehicle's position.

$$F_R = f_R \cdot m \cdot g \cdot \cos\alpha \qquad \text{Eq. (3)}$$

The gradient resistance is calculated with the downhill force using equation 4.

$$F_{St} = m \cdot g \cdot \sin\alpha \qquad \text{Eq. (4)}$$

The acceleration resistance force F_B describes the drag force of the entire vehicle due to its mass inertia during transient driving. The mass inertia is composed of a translational component due to the vehicle mass m and a rotational component due to the inertia of the rotating parts in the powertrain. Both components can be combined with the rotational mass factor e within the reduced vehicle mass m_{red} (Braess und Seiffert 2013). The acceleration a results as the time derivative of the speed v. Equation 5, 6 and 7 show the context:

$$F_B = m_{red} \cdot a \qquad \text{Eq. (5)}$$

$$m_{red} = m \cdot e \qquad \text{Eq. (6)}$$

$$a = \dot{v} = dv/dt \qquad \text{Eq. (7)}$$

The drag resistance force of the drive train F_A denotes the force at the wheel to keep the disengaged drive train in motion. F_A can be calculated according to equation 8 from the drag torque M_A at the wheel hub and the dynamic rolling radius r_{dyn}. The dynamic rolling radius is determined dynamically during the test from the speed v and the wheel speed n_A of the rear axle according to equation 9. Any slip that occurs is neglected.

$$F_A = M_A \cdot r_{dyn} \quad \text{Eq. (8)}$$

$$r_{dyn} = \frac{v}{2 \cdot \pi \cdot n_A} \quad \text{Eq. (9)}$$

The rolling resistance force F_R is determined from the balance of forces during coasting. No driving force acts to overcome the total resistance force F_{FW} through the drive train (equation 10). The rolling resistance force is therefore calculated according to equation 11 as the negative sum of the other driving resistance forces.

$$F_{FW} = 0 \Leftrightarrow 0 = F_L + F_R + F_{St} + F_B + F_A \quad \text{Eq. (10)}$$

$$F_R = -F_B - F_L - F_{St} - F_A \quad \text{Eq. (11)}$$

Using the drag forces from equations 2 to 5 and 8, and the acceleration α as the time derivative of the speed (equation 7), equation 11 is solved for the rolling resistance coefficient f_R in the next step (equation 12, 13, and 14):

$$f_R \cdot m \cdot g \cdot \cos\alpha = -m_{red} \cdot a - c_W \cdot A \cdot \frac{\rho_L}{2} \cdot v^2 - m \cdot g \cdot \sin\alpha - \frac{M_A \cdot v}{2 \cdot \pi \cdot n_A} \quad \text{Eq. (12)}$$

$$f_R = \frac{-m \cdot e \cdot a - c_W \cdot A \cdot \frac{\rho_L}{2} \cdot v^2 - m \cdot g \cdot \sin\alpha - \frac{M_A \cdot v}{2 \cdot \pi \cdot n_A}}{m \cdot g \cdot \cos\alpha} \quad \text{Eq. (13)}$$

$$f_R = \frac{-e \cdot \frac{dv}{dt}}{g \cdot \cos\alpha} - \frac{c_W \cdot A \cdot \frac{\rho_L}{2} \cdot v^2}{m \cdot g \cdot \cos\alpha} - \tan\alpha - \frac{M_A \cdot v}{2 \cdot \pi \cdot m \cdot g \cdot \cos\alpha \cdot n_A} \quad \text{Eq. (14)}$$

This means that the rolling resistance coefficient f_R can essentially be formulated as a function of the actual speed v or the acceleration a as its time derivative, the wheel speed n_A and the gradient angle α. All these parameters can be calculated from a highly accurate GNSS (Global Navigation Satellite System) position signal as well as the transmission signals available via the CAN bus (equation 15). The parameters e, c_W, A and M_A are discussed in the following section.

$$f_R = f(v, n_A, \alpha) \quad \text{Eq. (15)}$$

Test setup

An institute-owned tractor (John Deere 6210R) was used as a test vehicle for the coast-down tests. The tractor was equipped with measurement technology for recording the vehicle's internal electronic data communication via CAN bus. At the same time, the external data of the GNSS system was recorded via this measurement system. The Trimble AgGPS 542 RTK GNSS system with a mobile reference station was used to record the speed and gradient angle during the tests precisely. Position determination was thereby carried out with an accuracy of 1 cm horizontally (position) and 1.5 cm vertically (height) (Trimble 2014). Radial tires of the dimension 710/70 R 42 (Goodyear Optitrac R+) were mounted on the rear axle. The front tires with the dimension 600/70 R 28 were of the same model. The profile height was uniformly over 90% for all four tires. The design speed limit of the vehicle was 40 km/h. The values for aerodynamic drag required in equation 2 were conservatively estimated as $c_W = 1$. This assumption is permissible since the air resistance has a minor influence due to the low driving speed (Figure 4). The projected frontal area of the tractor of $A = 5.6$ m^2 was determined by image processing from the front view of the vehicle. The density of the air was assumed to be $\rho_L = 1.2$ kg/m^3. According to (Mitschke und Wallentowitz 2014) the torque mass factor $e = 1.05$ is for a truck with a mass of $m = 13$ t at an existing transmission ratio of i = 13. Due to the more complex design of the tractor transmission as a dual clutch transmission, the larger number of rotating parts in engagement and the greater rotational inertia of the wheels due to larger tire dimensions compared to truck tires, the torque mass factor $e = 1.2$ was used in the calculation. The drag torque M_A of the drive train was determined in a separate test. For this purpose, the tractor was positioned lifted up so that the wheels could rotate freely. A Lorenz DR2472 torque-speed sensor flanged to the wheel hub supplied the drag torque of the drive train with an external, stationary drive. The speed was varied via the imposed drive speed. A dependence of the wheel bearing friction on the wheel contact force, which is variable in driving operation, is generally neglected. By systematically determining the drag torque M_A via the speed and the gears of the transmission used in the test, it can be converted into a drag force of the drivetrain according to equation 8 and equation 9. Here, the dependence of the wheel bearing friction on the axle load is neglected. The empty mass of the tractor in the test was 8,750 kg and could be increased to a permissible total mass of 13,000 kg. The following ballasting options were available for the coast-down tests:

- Front weight (FG) 970 kg
- Rear weight 1 (HG1) 950 kg
- Rear weight 2 (HG2) 1,980 kg

In total, the tractor could be ballasted in six test variants with up to 3,900 kg at the front and rear. In order to determine the influence of the air pressure on the rolling resistance systematically, the tire pressure on all wheels was varied equally between 0.8 and 2.4 bar in steps of 0.4 bar for each test variant. Each test was repeated at least four times. Prior to the tests, the axle loads for each test variant were determined using a wheel load scale (WDi WWSD-15T, weighing range up to 15,000 kg, display accuracy 5 kg) at a tire pressure of 2.4 bar. The different test variants and the axle loads determined are shown in Table 1.

Table 1: Measured axle loads for different ballasting variants

Variant	RW1	RW2	RW3	RW4	RW5	RW6
Ballast front	-	FG	-	FG	-	FG
Ballast rear	-	-	HG1	HG1	HG1 + HG2	HG1 + HG2
Axle load front	3,560 kg	5,245 kg	3,095 kg	4,780 kg	1,520 kg	3,400 kg
Axle load rear	5,190 kg	4,480 kg	6,610 kg	5,940 kg	10,160 kg	9,430 kg
Axle load total	8,750 kg	9,725 kg	9,705 kg	10,720 kg	11,680 kg	12,830 kg
Relative axle load front	41%	54%	32%	45%	13%	27%
Relative axle load rear	59%	46%	68%	55%	87%	73%

A 900 m long track with an average gradient of 0.7% and a smooth asphalt surface was available for the coast-down tests at the Renningen test location (Figure 1). The test duration comprised four test days in September 2019. 308 individual coast-down tests were carried out. According to weather observations (German Weather Service), the average wind speed on all test days was about 1.2 m/s from a westerly direction parallel to the test track.

Figure 1: Smooth asphalt surface of the 900 m long test track (© J. Schwehn)

First, the tractor was accelerated to the maximum speed of 40 km/h in the forward direction of travel. After holding the speed for a short time, the direction selector lever was placed in the neutral position. The connection between the combustion engine and the wheels in the drive train is interrupted by opening the driving clutch. This marks the start of the coasting phase. The phase ends as soon as the vehicle comes to a halt and thus extends over the entire possible speed range of the vehicle. During the coasting phase, the parts of the drive train located between the driving clutch and the wheel hub continue to rotate. In the test tractor used, these include parts of the reversing transmission, the dual clutch transmission, the group transmission, the differential gears of both axles and the planetary gears of the final drives. In addition to the mass moment of inertia, the drag torque M_A, which leads to a braking effect on the wheels, is caused by the splash effects of structural elements running in oil and friction on seals and in bearings.

Figure 2 shows an example of the speed curve over time for variant RW6 with a tire pressure of 2.0 bar. Reaching the maximum speed and the subsequent decoupling process took place after 15 seconds shown in both cases. As the test track does not represent a perfect plane and the altitude profile is therefore different in the individual tests, the speed curves during coasting differ. When driving uphill, standstill was reached after about 67 s of coasting. Downhill, however, the vehicle came to a halt only after about 117 s.

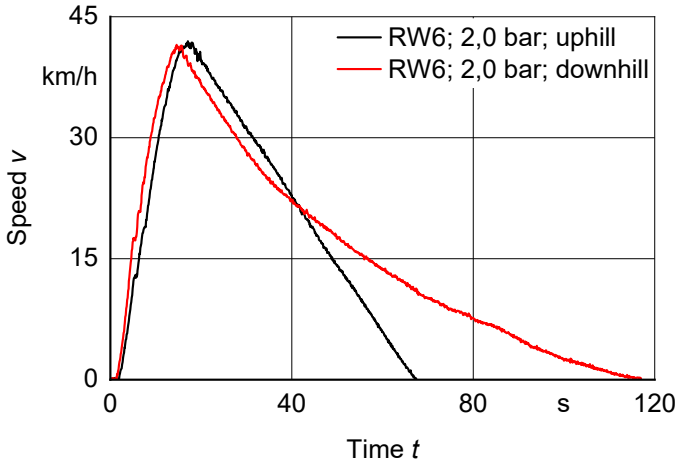

Figure 2: Speed curve over time for variant RW6 with 2.0 bar tire pressure and different track profiles

Figure 3 shows the time course of the gradient angle α for the same test configuration. The acceleration phase until the maximum speed is reached is not shown. The uphill journey is characterized by a majority positive gradient angle, the downhill journey by a predominantly negative gradient. The acceleration effect due to a sloping road led to a reduction in deceleration and thus to a prolongation of the coasting phase.

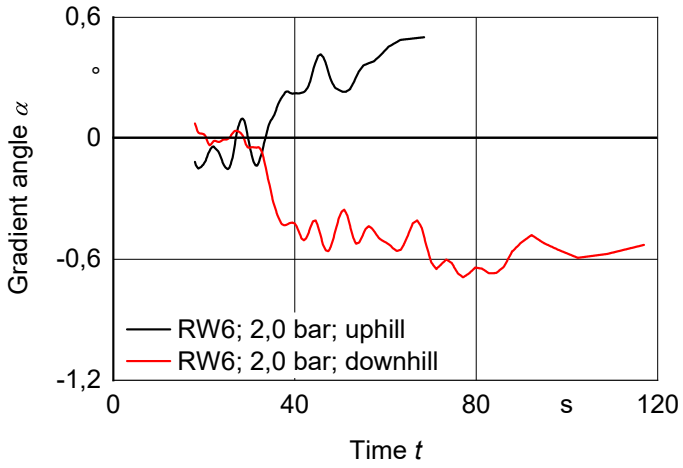

Figure 3: Gradient of the gradient angle α for variant RW6 with 2.0 bar tire pressure

As an example, Figure 4 shows the course of the individual driving resistances for the described test variants with the start of coasting. Modelling the driving resistances as a function of the acceleration a and the gradient angle α makes it possible to eliminate the influence of the elevation profile on the rolling resistance determination in the individual measurements. This allows the individual measurements to be treated as a ride on the horizontal plane and to be compared with each other, regardless of their elevation profile. This is achieved by correcting the acceleration resistance, which is only influenced by the acceleration a, for the driving resistances that depend on the gradient angle α. According to equation 11, the rolling resistance force F_R results from the negative sum of F_B, F_L, F_{St} and F_A. To illustrate the effect of the correction of the driving resistances on the rolling resistance, these resistance forces are therefore shown negatively in Figure 4.

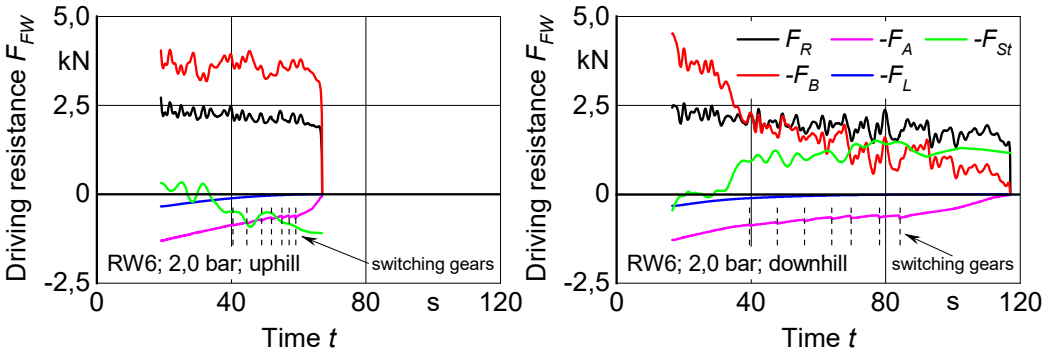

Figure 4: Course of driving resistances over time for variant RW6 with 2.0 bar

Compared with the other driving resistance forces, the influence of the air resistance force F_L is marginal due to the generally low driving speed, despite the quadratic relationship. The drag force from the gradient F_{St} is analogous to the gradient angle α from Figure 3. Due to the uphill travel, F_B is significantly larger than during the downhill travel, especially towards the end of the coasting phase. The topography of the coasting section has a clear influence on the coasting characteristics. Although the absolute values of the slope are consistently less than 1° (Figure 3), there is a significant influence on the deceleration. This pronounced sensitivity highlights the need to consider the slope as a modelling parameter and to correct it in the measured data (Figure 4). As expected, the drag force of the drive train F_A decreases continuously with speed, and the automatic shifting processes of the dual clutch transmission can be seen in both progressions. In the left-hand diagram of Figure 5, f_R is plotted against time. The result is a curve analogous to the rolling resistance force F_R from Figure 4. f_R is plotted against speed v, both cases show a very similar curve after taking the influence of the gradient into account, although the coasting time varies greatly.

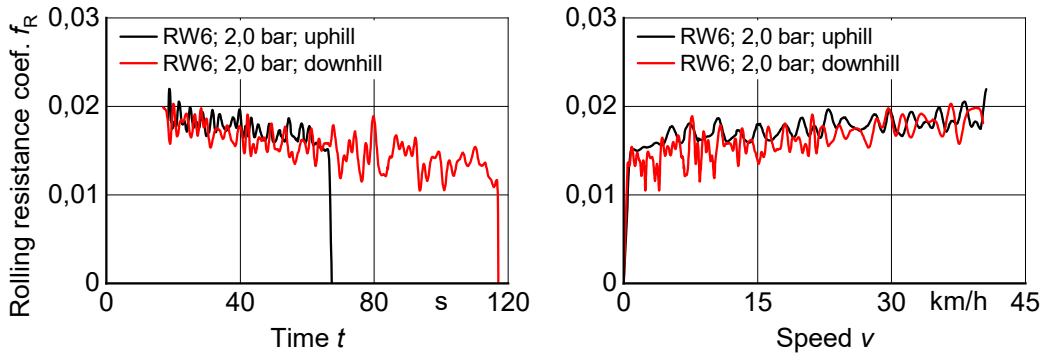

Figure 5: Rolling resistance coefficient when driving uphill and downhill, plotted against time and speed for variant RW6 with 2.0 bar tire pressure

Each test setting was repeated at least four times over the course using both driving directions, so that an average value can be calculated. The influence of tire and transmission oil temperature was effectively reduced by a warm-up phase. Figure 6 shows the rolling resistance coefficient f_R for eight repetitions and the resulting average value over the speed v. The standard deviation over each measurement point is 0.0012. The small scatter of the curves despite varying elevation profile for the individual measurements illustrates the effect of the gradient correction and supports the modelling approach presented. The curve of the rolling resistance coefficient f_R versus speed v, which can be seen in Figure 6 is characteristic for all the individual measurements carried out and agrees with the measurements of (Plesser 1997). At low speeds, a steep, degressive increase can be seen at first, which then continues above 3 km/h in a much flatter, linear manner. In the range of low speeds, the rolling resistance coefficient cannot be resolved more precisely with the method due to inaccuracies in the acceleration determination.

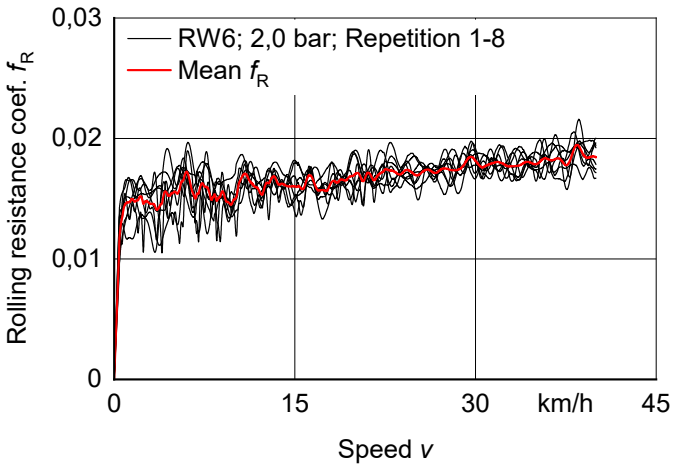

Figure 6: Averaging of the rolling resistance coefficient over eight repetitions

Test results

In the following presentation of the test results, the mean value curves of the rolling resistance coefficient f_R calculated over all repetitions of a test setting are used. These are plotted in a familiar way against the speed v. Figure 7 compares the different ballasting variants RW1 to RW6. Starting from variant RW1 without additional ballasting, the total weight is increased with weights in the front and rear linkage of the tractor (Table 1) up to full ballasting in variant RW6. All curves show the constant linear increase over speed. With the exception of RW3 and RW5 at low pressures, the increase occurs with a similar slope. As expected before, rolling resistance tends to increase with decreasing tire air pressure due to increasing deflection and increased flexing work. In the range of high air pressures of 1.6 to 2.4 bar, the curves generally exhibit only small distances. A reduction in tire pressure in this range does not lead to any significant change in tire deflection, so that the flexing loss work and thus the rolling resistance coefficient increase only slightly.

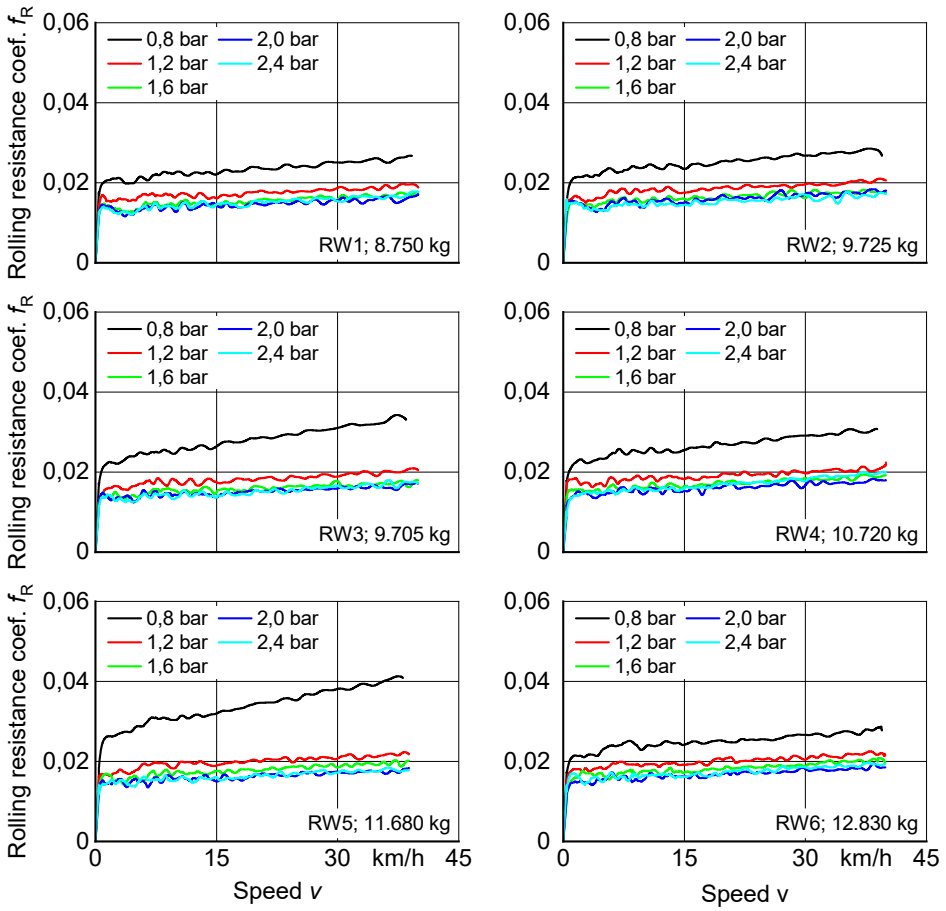

Figure 7: Comparison of rolling resistance coefficients for test variants RW1 to RW6 at a tire pressure of 0.8 to 2.4 bar

A further reduction in tire pressure below 1.6 bar causes a significant increase in the rolling resistance coefficient in all measurements. This can be explained by increased tire deformation because of increased tire deflection. The flexing loss work during rolling increases because the number of tire lugs in contact with the asphalt increases and the tire is more deformed. It is noticeable that from 1.2 to 0.8 bar there is a greater increase in rolling resistance than from 1.6 to 1.2 bar. This nonlinear influence of tire inflation pressure on the rolling resistance coefficient is evident for all configurations and is consistent with the experiments of Fery (2019) and Plesser (1997).

Discussion

The rolling resistance coefficient varies only slightly for tire pressures greater than 1.6 bar across the ballasting variants. For agricultural practice, it can be concluded from the measurements that lowering the tire inflation pressure in favour of comfort is possible for this tire, due to the small effect on the rolling resistance coefficient in the upper pressure range. It is assumed that the gain in comfort from reducing tire inflation pressure exceeds the disadvantage of slightly higher rolling resistance. The rolling resistance level is positively correlated with the total mass. At high tire pressures, a higher total mass has only a small effect on the rolling resistance. Particularly at the lowest tire pressure of 0.8 bar, a clear influence of the total mass is discernible. It can be seen that for all variants, rolling resistance increases with speed. A steeper increase is particularly noticeable at the

lowest tire pressure. Although the test variants RW3, RW5 and RW6 are very similar in terms of axle load distribution, rolling resistance varies significantly at 0.8 bar. On the one hand, f_R at RW5 reaches the maximum of the values measured in the test, although the total mass is below the maximum ballasting. On the other hand, the linear increase over speed is significantly more pronounced. Although RW6 represents a further increase in total mass compared to RW5, both the absolute rolling resistance coefficient and the linear increase are lower for 0.8 bar. Because of the further increase in total mass due to the full ballasting of the tractor, RW6 is expected to have a higher rolling resistance than RW4. This is true for all tire inflation pressures except 0.8 bar. Thus, the measured data for 0.8 bar give an impression of the influence of ballasting and axle load ratio on rolling resistance at very high axle loads. An influence of the axle load distribution can be assumed. The effect of a heavily loaded rear axle is clearly different from that of a heavily loaded front axle. From RW3 to RW4, the rear axle is relieved of 670 kg and the front axle is loaded by 1,685 kg. Although the load on the front axle is greater than the relief on the rear axle by a factor of 2.5, there is considerably less rolling resistance at RW4 than at RW3. In the case of RW5, this is particularly evident due to the axle load ratio of 13% front axle to 87% rear axle. Here, a noticeable increase in tire temperature was observed during the test, both in the tread and lug areas and in the tire sidewall. This is considered as an indication of excessive flexing loss work, which leads to a strong nonlinearity of the rolling resistance. This observation can be justified by the exceeding of the maximum tire load, which represents the existing wheel load in relation to the pressure-dependent maximum load that can be carried by the wheel. In principle, this variable is tire-dependent and varies considerably across all ballasting variants. In variant RW5, the maximum load capacity of the rear axle tires is exceeded by around 15%. However, the limited scope of the test with regard to the ballasting variants means that no further statement can be made about the influence of the axle load distribution and tire utilization.

Conclusions

Overall, the study shows that the coast-down test methodology coming from the passenger car sector can be applied to tractors. The method offers the advantage of being able to determine the rolling resistance of the entire vehicle or a tractor-trailer combination without the use of special tire measuring technology such as force measuring rims. For methodological reasons, it is not possible to determine the rolling resistance of individual tires. Due to the assumptions to be made for acceleration, drag and air resistance, it is only possible to determine the rolling resistance quantitatively in an idealized way. However, the method offers decisive advantages for comparative considerations. The high time efficiency additionally underlines the practical suitability. The user of the method is able to achieve a qualitative and quantitative comparison of different configurations of tire type, tire pressure and ballasting with little time and resources and without special tire measuring technology. Based on these findings, a suitable configuration can be selected and the total energy requirement for machine use can be optimized. Essential for the successful application of the presented methodology are a sufficiently long test track with consistent subsurface properties, access to the vehicle's CAN bus data and the use of a highly accurate GNSS system to determine the speed and gradient angle during the coast-down phase. Quantitative determination of the rolling resistance also requires knowledge of the drag of the powertrain and other vehicle-specific variables. The tests carried out on the example of the test tractor show a generally high repeatability and the need for gradient correction. Across all test variants, an increase in rolling resistance with increasing driving speed as well as a nonlinear

influence of tire air pressure due to the tire material are evident. The small effects on rolling resistance and thus fuel consumption in a range of 1.6 to 2.4 bar allow the recommendation to lower the tire pressure in practice for reasons of comfort. A more detailed analysis of the tests, primarily for low tire pressures, suggests itself. In addition to tire load, another possible explanation for the effects shown are different rolling resistances for front and rear axles, which are noticeable due to a varying distribution of the total weight on the axles. The limited ballasting possibilities within the scope of this investigation do not allow a closer examination of the influence of axle load distribution and tire utilization, since a separate variation of load distribution and total mass is not possible. In further investigations, moreover, the variance in terms of tire profile and design should be increased.

References

Barrelmeyer, T. (1994): Forces Acting on Driven Tractor Tyres with Stationary and Instationary Slip Angles, 28.–30.09.1994, Vienna, S. 238–262

Barrelmeyer, T. (1996): Untersuchung der Kräfte an gelenkten und angetriebenen Ackerschlepperrädern bei Gelände- und Straßenfahrt. Dissertation, Universität Stuttgart, Düsseldorf, VDI-Verlag

Bode, O.; Bode, M. (2013): Untersuchung des Rollwiderstands von Nutzfahrzeugreifen auf echten Fahrbahnen. FAT 255, S. 34

Braess, H.-H.; Seiffert, U. (Hg.) (2013): Vieweg Handbuch Kraftfahrzeugtechnik. Wiesbaden, Springer Vieweg, 7. Aufl.

Bundesministerium für Umwelt, Naturschutz und nukleare Sicherheit (BMU) (2019): Klimaschutz in Zahlen. Fakten, Trends und Impulse deutscher Klimapolitik. Broschüre, Berlin, 1. Aufl.

Decker, M.; Frerichs, L. (2016): Effiziente Kraftstoffnutzung in der AgrarTechnik - EKoTech. In: Jahrbuch Agrartechnik 2016. Hrsg. Frerichs, L., Braunschweig, Institut für mobile Maschinen und Nutzfahrzeuge. Hg. Frerichs, L., S. 22–29

Europäische Kommission (2018): Mitteilung der Kommission an das Europäische Parlament, den Rat, den Europäischen Wirtschafts- und Sozialausschuss und den Ausschuss der Regionen - Ein Rahmen für die Klima- und Energiepolitik im Zeitraum 2020–2030. Pressemitteilung, Brüssel (Belgien)

Heißing, B.; Ersoy, M.; Gies, S. (Hg.) (2013): Fahrwerkhandbuch. Grundlagen Fahrdynamik Komponenten Systeme Mechatronik Perspektiven. Wiesbaden, Springer Fachmedien, 4. Aufl.

Mitschke, M.; Wallentowitz, H. (2014): Dynamik der Kraftfahrzeuge. Wiesbaden, Springer Vieweg, 5. Aufl.

Plesser, J. (1997): Dynamisches Verhalten von Ackerschlepperreifen in Vertikal- und Längsrichtung auf fester Fahrbahn. Dissertation, Universität Stuttgart, Düsseldorf, VDI-Verlag

Reckleben, Y.; Schäfer, N.; Weißbach, M. (2013): Steigerung der Effizienz bei Straßentransporten mit unterschiedlichen Reifentypen für Traktoren. Landtechnik 68(3), S. 196–201, https://doi.org/10.15150/lt.2013.228

Schulze Zumkley, H. (2017): Reifenparameterermittlung aus Fahrversuchen mit einem Ackerschlepper unter besonderer Berücksichtigung des Hohenheimer Reifenmodells. Dissertation, Universität Stuttgart, Aachen, Shaker

Trimble (2014): TRIMBLE Ag-542 GNSS Receiver. Firmenschrift 022503-1301, Sunnyvale

VDMA e.V. (2017): Emissionsgesetzgebung für Mobile Maschinen: EU Stufe V – Fact Sheet. Broschüre VDMA e.V., Frankfurt am Main

Authors

M. Sc. Julian Schwehn and **M. Sc. Valentin Ernst** are research associates and **Prof. Dr.-Ing. Stefan Böttinger** is head of the Department of Fundamentals of Agricultural Engineering at the Institute of Agricultural Engineering at the University of Hohenheim, Garbenstr. 9, 70599 Stuttgart. E-mail:I: julian.schwehn@uni-hohenheim.de